

First Time Study of Magnetism and Ion Diffusion in Honeycomb Layered Oxide $\text{K}_2\text{Ni}_2\text{TeO}_6$ by Muon Spin Rotation

N. Matsubara,^{1,*} E. Nocerino,¹ O. K. Forslund,¹ A. Zubayer,¹ P. Gratex,² D. Andreica,³ J. Sugiyama,⁴ Z. Guguchia,⁵ S. Cottrell,⁶ A. Kalaboukhov,⁷ Y. Sassa,⁸ T. Masese,⁹ and M. Månsson^{1,†}

¹*Department of Applied Physics, KTH Royal Institute of Technology, SE-16440 Kista, Stockholm, Sweden*

²*Applied Electrochemistry, Department of Chemical Engineering, KTH Royal Institute of Technology, SE-10044, Stockholm, Sweden*

³*Faculty of Physics, Babe-Bolyai University, 400084 Cluj-Napoca, Romania*

⁴*Comprehensive Research Organization for Science and Society (CROSS), Tokai, Ibaragi 319-1106, Japan*

⁵*Laboratory for Muon Spin Spectroscopy, Paul Scherrer Institute, CH-5232 Villigen PSI, Switzerland*

⁶*ISIS Muon Facility, Rutherford Appleton Laboratory, Didcot, Oxfordshire, OX11 0QX, UK*

⁷*Microtechnology and Nanoscience, Chalmers University of Technology, SE-41296 Göthenburg, Sweden*

⁸*Department of Physics, Chalmers University of Technology, SE-41296 Göthenburg, Sweden*

⁹*Research Institute of Electrochemical Energy (RIECEN),*

National Institute of Advanced Industrial Science and Technology (AIST),

1-8-31 Midorigaoka, Ikeda, Osaka 563-8577, Japan

(Dated: September 1, 2022)

Investigation of potassium-ion (K^+) dynamics in materials using magneto-spin properties is an indomitable feat, due to its inherently weak nuclear magnetic moment relative to other lithophile ions such as sodium. On the other hand, spin-polarised muons in muon spin rotation and relaxation ($\mu^+\text{SR}$) measurements are known to have strong gyromagnetic moment ideal for probing dynamics of ions with weak magneto-spin moments in materials. Here we report the magnetic properties and K^+ dynamics in honeycomb layered oxide material using $\mu^+\text{SR}$ measurements. $\text{K}_2\text{Ni}_2\text{TeO}_6$ exhibits an antiferromagnetic transition at 26 K, as further affirmed by magnetic susceptibility measurements. Moreover, $\text{K}_2\text{Ni}_2\text{TeO}_6$ becomes antiferromagnetic under a first-order phase transition, with a possible commensurate spin ordering. $\mu^+\text{SR}$ studies performed on $\text{K}_2\text{Ni}_2\text{TeO}_6$ at high temperatures reveal potassium ions (K^+) to be mobile beyond 250 K (with an extrapolated activation energy of 120 (13) meV), revealing for the first time that K^+ dynamics in potassium-based materials can be measured using $\mu^+\text{SR}$.

I. INTRODUCTION

Layered oxides have garnered prime attention over the last decade owing to their piquant physical and chemical properties across varied aspects ranging from, *inter alia*, phase transition (e.g. superconductivity, Kitaev magnet)[1–4], thermodynamics (e.g. fast ionic conductivity) [5] and exotic electromagnetic spin interactions (multiferroics, high-voltage electrochemistry) [6–8]. Layered oxides entailing alkali atoms sandwiched between slabs with transition metal atoms (commonly referred to as transition metal layered oxides), have been at the cynosure of the aforementioned research endeavour. In particular, transition metal layered oxides adopting the chemical composition AMO_2 (where A denotes an alkali atom and M is typically a transition metal atom) have intensively been studied not only from a fundamental point of view but also an applied perspective. For instance, NaCoO_2 and its related compositions are a widely known material exhibiting a plenitude of intriguing physical properties at low temperatures such as spin density waves [9], superconductivity (hydrated compound [10, 11]), metal-insulator transitions [12], in addition

to unique magnetic and charge ordering phases [13].

In electrochemistry, NaCoO_2 has also been investigated as an electrode material (namely, cathode) in Na-ion batteries not only due to its sustainability but also its fast sodium-ion diffusive capabilities [14–16]. Despite this, another class of layered oxides has emerged to supersede NaCoO_2 , which comprises alkali atoms sandwiched between slabs with transition metal atoms now rearranged in a honeycomb fashion. Whilst both of these oxides admit a wide range of lithophile atoms such as Na, K, *et cetera*, the honeycomb framework endows e.g. $\text{Na}_2\text{Ni}_2\text{TeO}_6$ (or equivalently as $\text{Na}_{2/3}\text{Ni}_{2/3}\text{Te}_{1/3}\text{O}_2$) [17, 18] and $\text{K}_2\text{Ni}_2\text{TeO}_6$ ($\text{K}_{2/3}\text{Ni}_{2/3}\text{Te}_{1/3}\text{O}_2$) with a higher voltage cation electrochemistry and better structural stability [19]. $\text{K}_2\text{Ni}_2\text{TeO}_6$ adopts essentially the same crystal structural motif as $\text{Na}_2\text{Ni}_2\text{TeO}_6$ as shown in Figure 1(a), with a significant increase of the inter-slab distance owing to the larger potassium atoms that reside between the honeycomb slabs entailing Ni octahedra surrounding Te octahedra in a honeycomb fashion.

Exotic magnetic properties can be anticipated also in $\text{K}_2\text{Ni}_2\text{TeO}_6$, arising from the regular honeycomb configuration of Ni atoms (Figure 1(b)), triggering the interplay between adjacent antiferromagnetic (AFM) interactions [3, 18]. Complex magnetic structures can be expected owing to the competition between the direct interactions of magnetic Ni atoms and exchange interactions via the

* namim@kth.se

† condmat@kth.se

non-magnetic O atoms.

Besides, the large ionic radii of potassium cations which leads to the increase in the interslab distance influences not only their electric and magneto-spin interactions with Ni and O atoms, but also their diffusion properties. This is in part due to the weak nuclear magnetic moment of potassium and oxygen that mediates their interaction and consequently influences diffusion. Potassium, relative to other lithophile atoms such as sodium, has a weak nuclear magnetic moment that renders this interaction very elusive to probe.

This places muon spin rotation and relaxation (μ^+ SR) measurements at the frontier of spectroscopy techniques geared at probing the aforementioned interactions, since the positive muon possesses a charge and a strong gyromagnetic moment. In particular, the positive muon attaches to the negatively charged oxygen atoms whilst strongly interacting with the mobile cations. This means that diffusion of potassium cations with intrinsically weak magnetic interactions becomes feasible under μ^+ SR spectroscopy techniques. Here we report for the first time the measurement of magneto-spin and K-ion dynamics in honeycomb layered $\text{K}_2\text{Ni}_2\text{TeO}_6$ oxide material using μ^+ SR spectroscopy techniques. $\text{K}_2\text{Ni}_2\text{TeO}_6$ exhibits an antiferromagnetic transition at 26 K and ZF- μ^+ SR oscillation signal suggests commensurate spin ordering down to 2K. μ^+ SR studies performed on $\text{K}_2\text{Ni}_2\text{TeO}_6$ at high temperatures reveal potassium ions (K^+) to be dynamic above 250 K (with a measured activation energy of 120 (13) meV), revealing for the first time that K^+ dynamics can be effectively measured using μ^+ SR.

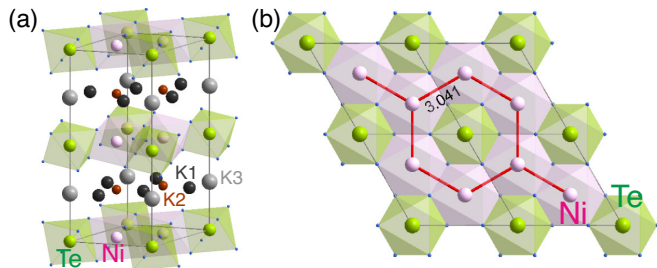


FIG. 1. Rendering of the honeycomb layered structure of $\text{K}_2\text{Ni}_2\text{TeO}_6$ showing the Ni atoms (pink), Te atoms (green), O atoms (blue) and K atoms occupying crystallographic sites (K1 (black), K2 (red), and K3 (gray)) that can move in a two-dimensional (2D) fashion, as reported in Ref.[19]. Red line indicates Ni-Ni network (interatomic distance in Å).

II. EXPERIMENTAL

A. Materials synthesis

Polycrystalline powders of $\text{K}_2\text{Ni}_2\text{TeO}_6(\text{K}_{2/3}\text{Ni}_{2/3}\text{Te}_{1/3}\text{O}_2)$ were synthesised us-

ing a high-temperature ceramics route. Stoichiometric amounts of NiO (99.9 % purity, Kojundo Chemical Laboratory (Japan)), TeO_2 (99.0 % purity, Aldrich) and K_2CO_3 (99.9% purity, Rare Metallic (Japan)) were mixed, pressed into pellets and finally heated for 23 h at 800°C in air. The attained powders were stored in an argon-purged glove box that was maintained at a dew point of below -80°C dP, to avert exposure of the materials to moisture.

B. Magnetic susceptibility measurements

Magnetic measurements (as a function of temperature) were performed with a 9 T Quantum Design superconducting quantum interference device magnetometer in zero-field-cooled (*zfc*) or field-cooled (*fc*) modes upon warming between 5 and 300 K. The magnetic susceptibility was obtained based on the equation $\chi = M/H$, where M is the magnetisation obtained by dividing the measured magnetic moment by the sample mass and H is the external applied magnetic field (in Oe).

C. Muon spin rotation and relaxation (μ^+ SR) measurements

μ^+ SR experiments were performed at a surface muon beam line using the surface muon spectrometer GPS at PSI in Switzerland. The powder sample ($m \approx 0.5$ g) was placed in a sealed envelope made out of a 25 μm -thick silver foil covering a surface area of $1 \times 1 \text{ cm}^2$. The sample preparation was performed in a helium glove-box to avoid sample degradation. In order to minimise the background signal, an envelope was attached to a fork-type Cu sample holder using a single layer of Al-coated mylar tape. The sample holder was attached to a stick and inserted into a liquid-He flow-type cryostat for measurements in the temperature ranges of 2 – 50 K where weak transverse-field (wTF) of 20 G, and zero-field (ZF) μ^+ SR spectra were collected.

For the high-temperature ion diffusion measurements, μ^+ SR spectra were recorded using a EMU spectrometer at the pulsed muon source of ISIS/RAL (UK). A powder sample of $\text{K}_2\text{Ni}_2\text{TeO}_6$ ($m \approx 1$ g) was pressed into a pellet with a diameter and thickness of 25 mm and 3.0 mm, respectively. This pellet was packed into a sealed (gold O-ring) powder cell made of non-magnetic titanium using a thin (50 μm) Ti-film window for the muons. Sample preparation was performed also inside a helium glove-box to avoid sample degradation. In addition, a silver mask was mounted onto the Ti-cell to ensure that no any minor background signal is non-relaxing in a wide temperature range. The cell was mounted onto a Cu end-plate of closed-cycle refrigerator (CCR) and measurements were performed at temperatures ranging between 50 and 550 K. μ^+ SR spectra were subsequently collected at ZF, wTF (of 20 G) and longitudinal field

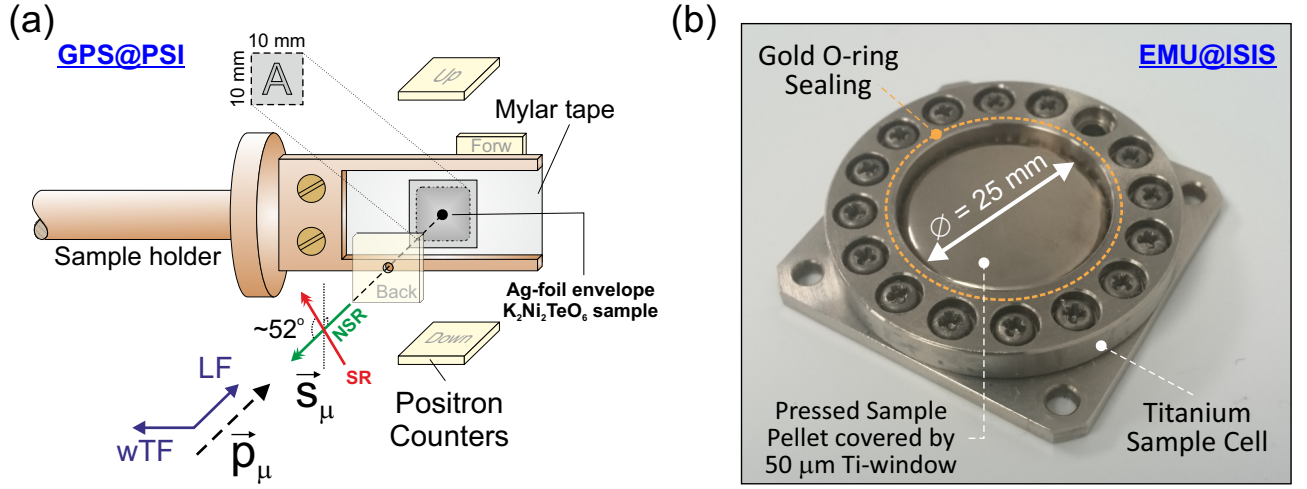


FIG. 2. (a) Illustration of the experimental setup used to perform magnetic muon spin rotation and relaxation (μ^+ SR) measurements at the GPS/PSI spectrometer. The muon is applied through the back detector to the sample, where \vec{P}_μ is the momentum vector of the muon and \vec{S}_μ the spin vector pointing away from the direction of motion. The muon attaches to the sample and subsequently decays into positrons, which are counted by the detectors, and neutrinos. LF denotes the longitudinal field whereas wTF is the weak transverse field applied to the muons. (b) Sealed and mounted titanium sample cell used for the μ^+ SR ion diffusion measurements at EMU/ISIS

(LF) of 10 and 30 G.

Details regarding the experimental techniques and setups are provided in Fig. 2 as well as in Ref. 20. The musrfit[21] software package was used to analyse the μ^+ SR data.

III. RESULTS AND DISCUSSION

A. Magnetic susceptibility

Figure 3 shows the *dc* magnetic susceptibility plots of $\text{K}_2\text{Ni}_2\text{TeO}_6$ measured under a magnetic field of 100 Oe in the temperature ranges of 5 - 300 K. $\text{K}_2\text{Ni}_2\text{TeO}_6$ exhibits antiferromagnetic behaviour with a maxima of the curve at around 33 K. The magnetic transition is also well evidenced in the differential susceptibility $[d\chi/dT](T)$ curves, at an antiferromagnetic Neel temperature (T_N) of approximately 26 K in both *zfc* and *fc* modes (only *fc* is shown in inset of Figure 3).

No significant divergence between *zfc* and *fc* magnetisation curves is observed. The susceptibility data ($1/\chi$) were fit to the Curie-Weiss (CW) law (using data points above 80 K), yielding a Curie-Weiss constant $\theta_{\text{CW}} = -30.3$ K. The negative Weiss constant indicates AFM interactions, which could arise from superexchange interaction of nearest and next-nearest neighbour interactions of Ni. Further, an effective magnetic moment, $\mu_{\text{eff}} = 2.53 \mu_B/\text{Ni}$ was obtained, which is in agreement with the theoretical spin only value for Ni^{2+} ($2.3 \mu_B$). The slight higher value of experimental magnetic moment can be explain by the

spin-orbital coupling as also mentioned in $\text{Na}_2\text{Ni}_2\text{TeO}_6$ [18, 22].

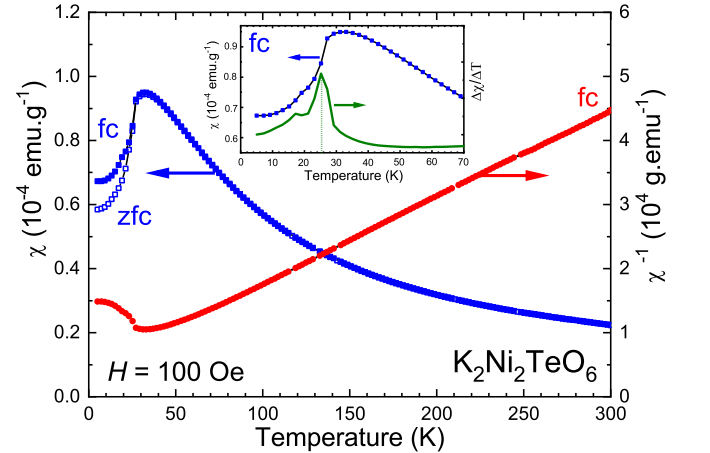


FIG. 3. Magnetic susceptibility ($\chi(T)$ and $1/\chi(T)$) curves of $\text{K}_2\text{Ni}_2\text{TeO}_6$ recorded in zero-field-cooled (*zfc*) and field-cooled (*fc*) modes at an applied magnetic field of 100 Oe. Inset shows the magnified image of the susceptibility plots highlighting no bifurcation of *zfc* and *fc* curves.

B. Low-temperature μ^+ SR measurements under a weak transverse field (wTF)

Figure 4(a) shows the variation in the wTF time spectra recorded at three different temperatures. When the

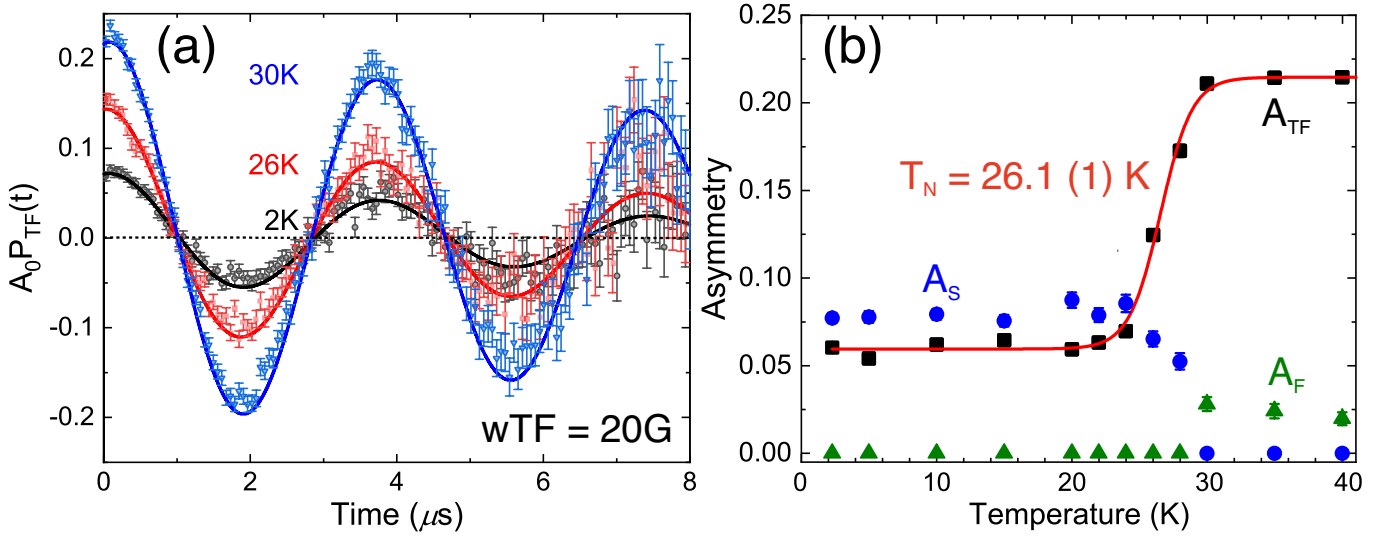


FIG. 4. (a) μ^+ SR spectra as a function of time taken at temperatures of 2 K, 26 K and 30 K under a weak-transverse field (wTF) of 20 G, and the corresponding fits using Eq. 1. For clarity, A_0 is the initial asymmetry and $P_{TF}(t)$ is the muon spin polarisation function. (b) Asymmetry plots as functions of temperature, where A_{TF} , A_S and A_F are the asymmetries of the related polarisation components. The sigmoid fit is indicated as a red solid line, with the antiferromagnetic transition temperature (T_N) at 26.1 K.

temperature decreases below 30 K, the oscillation amplitude due to the applied wTF rapidly decreases, indicating the appearance of additional internal magnetic fields (i.e. static spin order). Below 30 K, the wTF μ^+ SR spectrum was consequently fitted using a combination of a relaxing precessing signal and a slow relaxing non-oscillatory signal. The first component is due to the externally applied magnetic field (wTF = 20 G) and the second due to the internal magnetic field induced from the magnetic ordering. Above 30 K, the spectrum was fitted using a combination of a relaxing precessing signal and a fast relaxing non-oscillatory signal due to the fast spin fluctuation. The fit function for the wTF spectra is as follows:

$$A_0 P_{TF}(t) = A_{TF} \cos(2\pi\omega_{TF}t + \phi_{TF}) \cdot \exp(-\lambda_{TF}t) + A_S \cdot \exp(-\lambda_S t) + A_F \cdot \exp(-\lambda_F t), \quad (1)$$

where $P_{TF}(t)$ is the muon spin polarisation function, A_0 is the initial asymmetry, A_{TF} , A_S and A_F are the asymmetries of the related polarisation components, $2\pi\nu_{TF}$ is the angular frequency of the Larmor precession under applied transverse field, λ_{TF} , λ_S and λ_F are the exponential relaxation rates for the three components and ϕ is the initial phase of the processing signal.

The magnetic transition temperature can be determined by analysing the fitting parameter A_{TF} . An increase of the A_{TF} fits is observed as the temperature increases, corresponding to a transition from a magnetically ordered state to a paramagnetic state. As shown in Figure 4 (b), the trend of the asymmetries has been fitted with a sigmoid fit and the transition temperature is defined as the middle point of the fitting curve, where the

normalised $A_{TF}/A_0 = N_{ATF}$ is equal to 0.5. The bulk magnetic transition defined by μ^+ SR is $T_N = 26.1$ (1) K. This transition temperature is in excellent agreement with the result from magnetisation measurement (Figure 3).

Below 20 K down to the base temperature of this experiment (2 K), the oscillation from the externally applied field is still observed clearly, volume fraction of 28 %, corresponding to a paramagnetic phase. This could suggest the presence of a second paramagnetic phase in this compound, which might have a magnetic transition at even lower-temperature. However, it could also indicate the presence of a high-symmetry muon site where the resulting internal magnetic field is zero down to $T = 2$ K. The absence of any detectable impurity phases from X-ray diffraction measurements, clearly supports the latter case.

C. μ^+ SR measurements under zero-field (ZF) taken below antiferromagnetic transition temperature (T_N)

To further understand the magnetic ordering of $K_2Ni_2TeO_6$, μ^+ SR measurements under zero-field were performed at temperatures between 2 and 40 K. Figure 5 shows time spectra recorded at base temperature 2 K. It is apparent that muon spins are precessing at 2 K due to the appearance of a spontaneous internal magnetic field, resulting in a clear oscillation in the time spectrum under ZF. This is a typical response from a muon ensemble in a magnetically ordered state. Inset of Figure 5 shows

the time spectrum under ZF at 2 K in an early time domain for $\text{K}_2\text{Ni}_2\text{TeO}_6$. Fourier analysis of the signal reveals two distinct components with frequencies: $f_{\text{AF1}} = 30$ MHz and $f_{\text{AF2}} = 43$ MHz, with an asymmetry ratio of 1 : 10 (as is shown in Figure 7(d)).

In addition, there is a fast relaxing signal in the initial time spectra. Such behaviour may have several explanations; in particular this kind of signal might be due to delocalised muons or fast fluctuating moments arising from either the Ni ions or magnetic impurities. Thus, this ZF spectrum at 2 K was fitted by a combination of two damped cosine oscillations, which are originating from the static magnetic ordered, one fast and one slow (for 1/3 tail) exponentially relaxing non-oscillatory components and one exponentially relaxing non-oscillatory components due to the paramagnetic signal observed by wTF spectra (A_{BG} fixed at 0.0728):

$$\begin{aligned} A_0 P_{\text{ZF}}(t) = & A_{\text{AF1}} \cos(\omega_{\text{AF1}} + \phi_{\text{AF1}}) \cdot \exp(-\lambda_{\text{AF1}} t) \\ & + A_{\text{AF2}} \cos(\omega_{\text{AF2}} + \phi_{\text{AF2}}) \cdot \exp(-\lambda_{\text{AF2}} t) \\ & + A_{\text{F}} \cdot \exp(-\lambda_{\text{F}} t) \\ & + A_{\text{tail}} \cdot \exp(-\lambda_{\text{tail}} t) \\ & + A_{\text{BG}} \cdot \exp(-\lambda_{\text{BG}} t), \end{aligned} \quad (2)$$

where A_0 is the initial asymmetry, A_{AF1} , A_{AF2} , A_{S} , and A_{F} are the asymmetries associated with the four signals, ω_{AF} is the angular frequency of the muon spin precession corresponding to the static internal AF field, ϕ_{AF1} is the initial phase of the oscillatory signal, λ_{AF} , λ_{S} , and λ_{F} are the exponential relaxation rates of each signal.

As shown in Figure 5, both short ($t < 0.2 \mu\text{s}$) and long (t up to $8 \mu\text{s}$) time spectra were well fitted using Eq. 2.

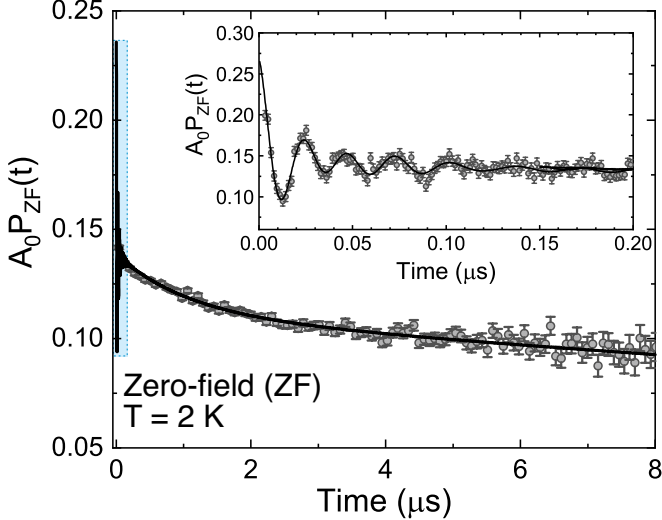


FIG. 5. $\mu^+\text{SR}$ time spectrum at a temperature of 2 K under zero-field (ZF). The inset shows a shorter time domain where the muon spin precession is evident. The solid lines are the fits of the respective ZF functions [Eq. 2] to the data.

Both ϕ_{AF1} and ϕ_{AF2} show similar temperature trend from individual fitting, thus the ϕ_{AF} values were fixed

to be same. The A_{AF1} and A_{AF2} values were also found to be more or less independent of the temperature, that is 0.0065 and 0.0811 respectively, and were treated as common parameters in the temperature range between 2 and 23.5 K.

Figure 6 shows the temperature dependency of ZF- $\mu^+\text{SR}$ time spectra ($t < 0.2 \mu\text{s}$) in between 2 and 30 K. The time spectra recorded below the transition temperature ($= 26$ K) were well fitted using the Eq. 2 in both long and short time domains. Figure 7(a) exhibits the two frequencies as a function of temperature, corresponding to a magnetic order parameter. As temperature decreases from 40 K, both f_{AF1} and f_{AF2} drastically increase ($\sim 75 - 93$ % of its base temperature value) at around 25 K. This is indicative of a first-order transition, which then could be linked to a multiple structural phase transition. Furthermore, these two frequencies seem to abruptly disappear almost at the same temperature (namely, $T_{\text{N}} = 26$ K). This suggests that the two frequencies are not caused by the coexistence of two different phases in the sample but rather by two magnetically inequivalent muon sites in the lattice. Both λ_{AF1} and λ_{AF2} are rather constant (Figure 7(b)), but the λ_{AF2} increases near T_{N} , indicating an increase towards a wider field distribution around T_{N} .

Finally, except for a small temperature range near T_{N} , ϕ_{AF} is -20° at 2 K and is almost constant up to the vicinity of T_{N} (Figure 7(c)). This suggests that Eq. 2, that models a commensurate spin structure to the crystal structure lattice period, might be too simple. Instead some form of incommensurate spin order could perhaps be expected, given that incommensurate spin order results in a shift of the time spectrum. In such cases a combination of spherical Bessel function, that models incommensurate ordering, might be more suitable. Indeed, usually a commensurate magnetic ordering gives $\phi_{\text{AF}} = 0$, but small phase shifts in AF are not too uncommon. Finally, this -20° delay could also be emanating from the presence of multiple muon sites. [23, 24].

Note that all the $\mu^+\text{SR}$ parameters under ZF show a monotonic change in the temperature range between 2 K and T_{N} . The present results hence suggest the absence of an additional magnetic transition in this temperature range, which is in good agreement with the magnetisation and wTF spectra results. Neutron diffraction studies can shed light on the magnetic order of $\text{K}_2\text{Ni}_2\text{TeO}_6$, details of which are beyond the scope of the current study.

D. High-temperature potassium-ion diffusive properties

To study the solid-state K-ion diffusive properties of $\text{K}_2\text{Ni}_2\text{TeO}_6$ compound, $\mu^+\text{SR}$ measurements above the magnetic transition temperature were performed. Both Li-ion [25–27] and Na-ion [28, 29] diffusive properties as a function of temperature have been extensively studied using a series of ZF, wTF and LF $\mu^+\text{SR}$ time spectra

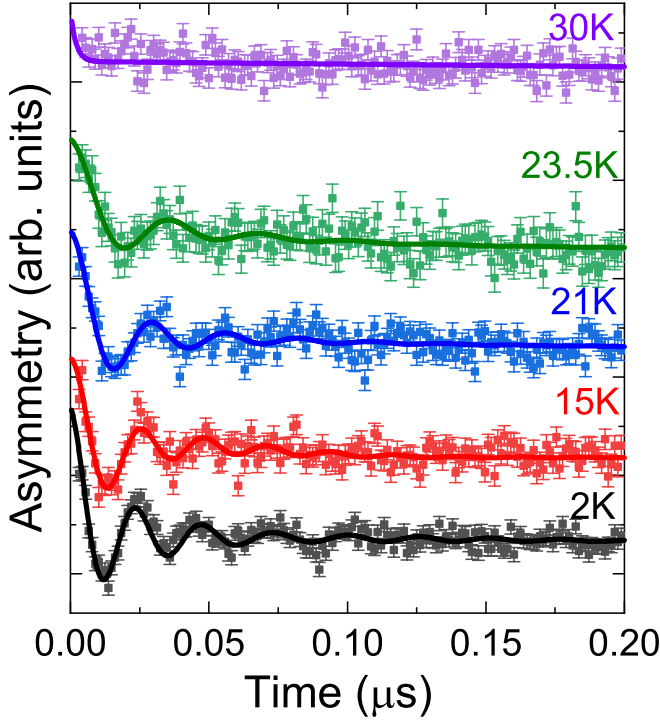


FIG. 6. Temperature-dependent μ^+ SR spectra for $\text{K}_2\text{Ni}_2\text{TeO}_6$ taken under zero-field. Solid lines show the fits based on Eq. 2. Each spectrum was offset along the y-axis by 0.1, for clarity of display.

and standard techniques such as nuclear magnetic resonance (NMR) spectroscopy. However, since the nuclear moment of K ($\mu[^{39}\text{K}] = 0.39 \mu_N$) is much smaller than for Li ($\mu[^7\text{Li}] = 3.26 \mu_N$) and Na ($\mu[^{23}\text{Na}] = 2.22 \mu_N$), the measurement of K-ion dynamics using standard techniques [30, 31] is challenging. This means that μ^+ SR is uniquely suited to probing the K-ion diffusive properties.

In what follows, μ^+ SR time spectra were collected in the temperature range between 50 and 550 K at EMU, (ISIS, UK). At each temperature, the ZF and two LF spectra (10 and 30 G) were fitted by two exponentially relaxing dynamic Kubo-Toyabe (KT) function and a background signal from the fraction of muons stopped mainly in the silver plate mask:

$$A_0 P_{\text{LF}}(t) = A_{\text{KT1}} G^{\text{DGKT}}(\Delta_1, v_1, t, H_{\text{LF}}) \cdot \exp(-\lambda_{\text{KT1}} t) + A_{\text{KT2}} G^{\text{DGKT}}(\Delta_2, v_2, t, H_{\text{LF}}) \cdot \exp(-\lambda_{\text{KT2}} t) + A_{\text{BG}}, \quad (3)$$

where A_0 is the initial asymmetry, A_{KT} and A_{BG} are the asymmetries associated with the two signals, Δ is related to the static width of the local field distribution at the disordered sites via the gyromagnetic ratio of the muons, and ν is the field fluctuation rate. When $\nu = 0$, and $H_{\text{LF1}} = 0$, $G^{\text{DGKT}}(\Delta_1, v_1, t, H_{\text{LF1}})$ is the static Gaussian KT function in ZF. Furthermore, a fitting procedure was employed over the entire temperature range using a

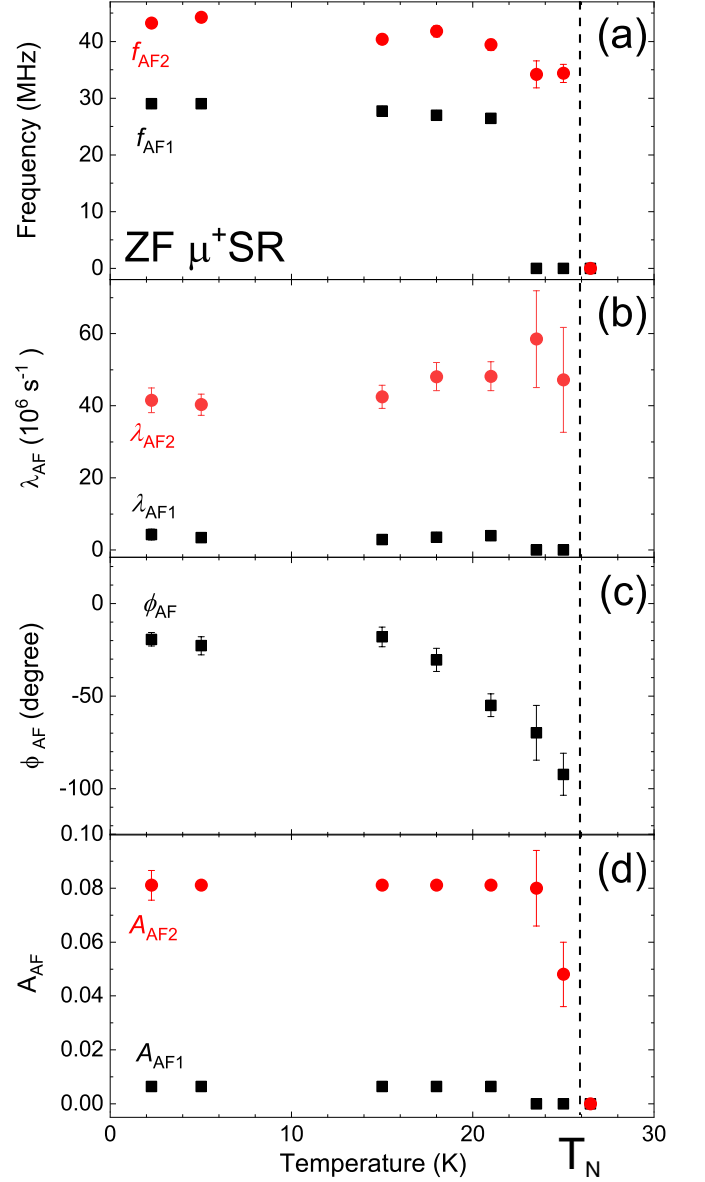


FIG. 7. Temperature dependencies of μ^+ SR parameters taken for $\text{K}_2\text{Ni}_2\text{TeO}_6$; (a) muon-spin precession frequencies ($f_{\text{AF}} = \omega_{\text{AF}}/2\pi$), (b) the relaxation rates (λ_{AF}), (c) the initial phases of the two oscillatory signals (ϕ_{AF}) and (d) the asymmetries (A_{AF}). The data were obtained by fitting the ZF spectra using Eq. 2. Vertical dashed line indicates the antiferromagnetic transition temperature $T_N \approx 26$ K.

common background asymmetry ($A_{\text{BG}} \sim 0.04723$), but with a temperature dependent field fluctuation rate (ν) and relaxation rate (λ). Δ was also treated as a common parameter over the entire temperature range [$\Delta_{\text{KT1}} \sim 0.0432 \text{ s}^{-1}$ and $\Delta_{\text{KT2}} \sim 0.291 \text{ s}^{-1}$]. Since the two Δ_{KT} are one order magnitude different, this means two individual muon sites with the different local field distribution in the lattice. The volume fraction ratio between $A_{\text{KT1}}/A_{\text{KT2}}$ is 6/4 at 50 K while 32/1 at 550 K as shown

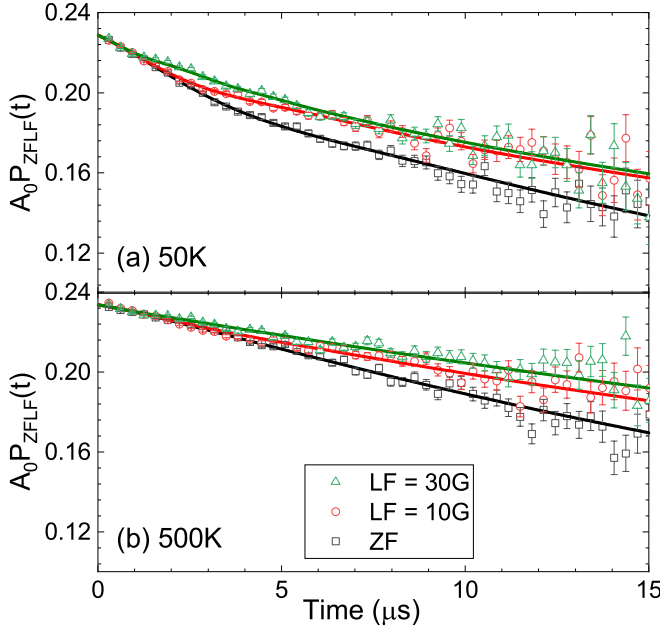


FIG. 8. ZF and two LF (10 and 30 G) μ^+ SR spectra for measured at (a) 50 K and (b) 500 K. Solid lines represent the fit result using Eq. 3

in Figure 9(a). Two muon sites are also observed in the μ^+ SR study (Eq. 2). However, in order to investigate the location and number of muon site in the lattice, theoretical calculations based on the crystal structure model is required. Figure 8 shows the ZF and longitudinal field (LF) μ^+ SR time spectrum obtained at (a) 50 K, (b) 500 K. A decoupling effect by the applied LF (= 10 and 30 G), i.e. a reduction in the relaxation rate, is seen even for small fields even at 50 K, suggesting that the depolarisation seen in Fig. 8 (a) is stemming from nuclear moments. The small nuclear moments of the compound elements (K, Ni, Te and O) in the compound result in small values of Δ , resulting in a almost exponential like line shape.

Figure 9 (c) shows the temperature dependency of ν from two KT functions. ν_{KT1} is almost constant over whole temperature range (ν_{KT1} at 50 K is 0.184), while ν_{KT2} is close to zero up to 200 K, and start increasing at 250 K. The increase in ν_{KT2} between 250 and 550 K can be explained by a thermal activation process, which signals the onset of diffusive motion of either K^+ or μ^+ above 250 K. Here, the scenario of K-ion diffusion is strongly supported by electrochemical investigations that clearly indicate that the K-ions are mobile at these temperatures. The $\nu_{KT2}(T)$ of $K_2Ni_2TeO_6$ can be fitted to an Arrhenius type equation [red dashed line in Fig. 9]. From such fit, it is possible to extract the activation energy, which yield $E_a = 120$ (13) meV. Note that ν_{KT2} for $T > 500$ K is excluded for this Arrhenius relationship since the error bar is large compare to the other temperature points.

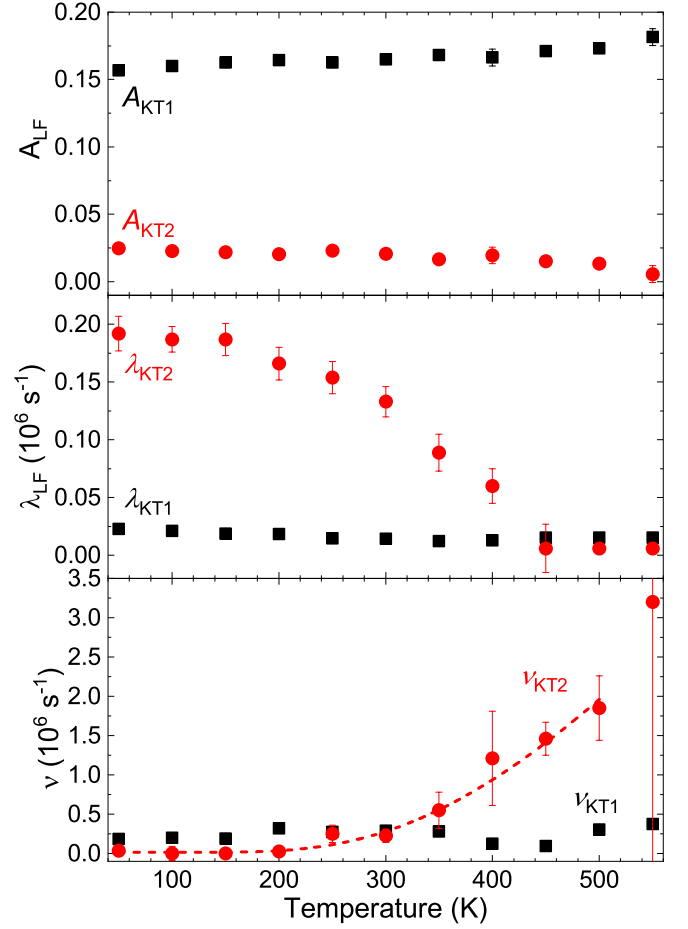


FIG. 9. The temperature dependencies of (a) the asymmetry (A_{KT}), (b) λ_{KT} and (c) ν_{KT} for $K_2Ni_2TeO_6$. The red dashed line is fit to an Arrhenius equation $\nu = A \cdot \exp(-E_a/k_B T)$, which yield an activation energy of $E_a = 120(13)$ meV. Each data point was obtained by fitting the ZF and LF (= 10 and 30 G) spectra using Eq. 3.

Finally, we can estimate the K-ion diffusion coefficient D_K using the obtained fluctuation rate ν as directly measuring the ion hopping rate. The field fluctuation rate has in the past been successfully used to determine the diffusion coefficient for Li and Na compounds [26],[29]. The principle of diffusion should naturally not change between the ions and similar calculation can then be done for K^+ . Assuming that the increase in ν [see Fig. 9(c)] is due to K-ion diffusion, D_K can be estimated via

$$D_K = \sum_{i=1}^h \frac{1}{N_i} Z_{v,i} s_i^2 \nu, \quad (4)$$

where N is the number of K sites, Z is the vacancy fraction and s is the jump distance. Naturally, we shall restrict the diffusion path within the 2D layer of the honeycomb. Moreover, for simplicity, we shall naively assume a diffusion path only within the nearest neighbour sites within the honeycomb flower, giving $Z_{adv} = 0.24$,

$s_{\text{adv}} = 1.71 \text{ \AA}$ and $N = 3$. Such assumption yields $D = 1.8606 \times 10^{-11} \text{ cm}^2/\text{s}$ for $\nu(300\text{K}) = 0.29 \times 10^{-6}$. This value is one order of magnitude lower than the value of LiCoO_2 [26]. D_K can also be calculated for other temperatures, e.g. $9.0053 \times 10^{-11} \text{ cm}^2/\text{s}$ using $\nu(400\text{K}) = 1.21 \times 10^{-6}$ and $1.3768 \times 10^{-10} \text{ cm}^2/\text{s}$ using $\nu(500\text{K}) = 1.85 \times 10^{-6}$. Here it is assumed that the atomic structure remains the same within the entire temperature range.

To further investigate the ion diffusion in $\text{K}_2\text{Ni}_2\text{TeO}_6$, detailed studies of the temperature dependent atomic structure using X-ray and/or neutron diffraction will be needed. Such investigations could also yield a more accurate information on the active diffusion paths [32], which would also make our calculations of D_K from $\nu(T)$ much more reliable.

IV. CONCLUSIONS

Muon spin rotation and relaxation ($\mu^+\text{SR}$) measurements on $\text{K}_2\text{Ni}_2\text{TeO}_6$ reveal the onset of commensurate-like antiferromagnetic transitions at 26 K, which is of a first-order. Further, potassium-ions (K^+) in $\text{K}_2\text{Ni}_2\text{TeO}_6$ have been found to be mobile above 250 K, with remarkably low activation energy of 120 (13) meV which is comparable to thermal activation energy scales of related lithium- and sodium-based materials. This brings related honeycomb layered oxide materials to the foreground of fast ionic conductors for energy storage. Moreover, we have shown, for the first time, the

feasibility of $\mu^+\text{SR}$ study in investigating the K^+ dynamics of materials which tend to have low nuclear magnetic moments. This study expands the research frontier of alkali-ion dynamics within materials, previously relegated mainly to lithium and sodium.

V. ACKNOWLEDGEMENTS

This research was supported by the European Commission through a Marie Skłodowska-Curie Action and the Swedish Research Council - VR (Dnr. 2014-6426 and 2016-06955) as well as the Carl Tryggers Foundation for Scientific Research (CTS-16:324). J.S. acknowledge support from Japan Society for the Promotion Science (JSPS) KAKENHI Grant No. JP26286084 and JP18H01863. Y.S. is funded by the Swedish Research Council (VR) through a Starting Grant (Dnr. 2017-05078) and E.N. the Swedish Foundation for Strategic Research (SSF) within the Swedish national graduate school in neutron scattering (SwedNess). D.A. acknowledges partial financial support from the Romanian UEFISCDI project PN-III-P4-ID-PCE-2016-0534. T.M. acknowledges the National Institute of Advanced Industrial Science Technology (AIST), Japan Society for the Promotion of Science (JSPS KAKENHI Grant Numbers 19 K15685) and Japan Prize Foundation. Finally, the authors are grateful to the Paul Scherrer Institute and ISIS/RAL for the allocated muon beam-time as well as the great support from their technical staff.

-
- [1] N. Matsubara, S. Petit, C. Martin, F. Fauth, E. Suard, S. Rols, and F. Damay, *Physical Review B* **100**, 2 (2019).
 - [2] C.-H. H. Lee, C.-W. W. Wang, Y. Zhao, W.-H. H. Li, J. W. Lynn, A. B. Harris, K. Rule, H.-D. D. Yang, and H. Berger, *Scientific Reports* **7**, 6437 (2017).
 - [3] S. K. Karna, Y. Zhao, R. Sankar, M. Avdeev, P. C. Tseng, C. W. Wang, G. J. Shu, K. Matan, G. Y. Guo, and F. C. Chou, *Physical Review B* **95**, 1 (2017).
 - [4] S. W. Kim, Z. Deng, M.-R. Li, A. S. Gupta, H. Akamatsu, V. Gopalan, and M. Greenblatt, *Inorg. Chem.* **55**, 1333 (2016).
 - [5] Z. Yang, Y. Jiang, L. Deng, T. Wang, S. Chen, and Y. Huang, *Journal of Power Sources* **360**, 319 (2017).
 - [6] N. D. Khanh, N. Abe, H. Sagayama, A. Nakao, T. Hanashima, R. Kiyonagi, Y. Tokunaga, and T. Arima, *Physical Review B* **93**, 1 (2016).
 - [7] S. Chaudhary, P. Srivastava, and S. Patnaik, *AIP Conference Proceedings* **1942**, 2 (2018).
 - [8] S. Choi, S. Manni, J. Singleton, C. V. Topping, T. Lancaster, S. J. Blundell, D. T. Adroja, V. Zapf, P. Gegenwart, and R. Coldea, *Physical Review B* **99**, 1 (2019), [arXiv:1810.03212](#).
 - [9] J. Wooldridge, D. Mck Paul, G. Balakrishnan, and M. R. Lees, *Journal of Physics Condensed Matter* **17**, 707 (2005), [arXiv:0406513v2 \[arXiv:cond-mat\]](#).
 - [10] R. E. Schaak, T. Klimczuk, M. L. Foo, and R. J. Cava, *Nature* **424**, 527 (2003).
 - [11] K. Takada, M. Onoda, Y. N. Choi, D. N. Argyriou, F. Izumi, H. Sakurai, E. Takayama-Muromachi, and T. Sasaki, *Chemistry of Materials* **21**, 3693 (2009).
 - [12] J. Sugiyama, J. H. Brewer, E. J. Ansaldi, H. Itahara, T. Tani, M. Mikami, Y. Mori, T. Sasaki, S. Hébert, and A. Maignan, *Physical Review Letters* **92**, 4 (2004), [arXiv:0310516 \[cond-mat\]](#).
 - [13] J. T. Hertz, Q. Huang, T. McQueen, T. Klimczuk, J. W. Bos, L. Viciu, and R. J. Cava, *Physical Review B - Condensed Matter and Materials Physics* **77**, 1 (2008).
 - [14] G. M. Alexander, R. E. Allen, A. Atala, W. Bowen, A. A. Coley, J. B. Goodenough, M. I. Katsnelson, E. V. Koonin, M. Krenn, L. S. Madsen, M. Månsson, N. P. Mauranyapin, A. I. Melvin, E. M. Rasel, L. E. Reichl, R. Yampolskiy, P. B. Yasskin, A. Zeilinger, and S. Lidstrom, *Physica Scripta* (2020), [10.1088/1402-4896/ab7a35](#).
 - [15] B. V. Rami Reddy, R. Ravikumar, C. Nithya, and S. Gopukumar, *Journal of Materials Chemistry A* **3**, 18059 (2015).
 - [16] A. K. Rai, L. T. Anh, J. Gim, V. Mathew, and J. Kim, *Ceramics International* **40**, 2411 (2014).
 - [17] A. Gupta, C. Buddie Mullins, and J. B. Goodenough, *Journal of Power Sources* **243**, 817 (2013).
 - [18] R. Berthelot, W. Schmidt, A. W. Sleight, and M. A. Subramanian, *Journal of Solid State Chemistry* **196**, 225 (2012).

- [19] T. Masese, K. Yoshii, Y. Yamaguchi, T. Okumura, Z. D. Huang, M. Kato, K. Kubota, J. Furutani, Y. Orikasa, H. Senoh, H. Sakaebe, and M. Shikano, *Nature Communications* **9**, 1 (2018).
- [20] A. Yaouanc and P. D. De Réotier, *Muon Spin Rotation, Relaxation, and Resonance Applications* (Oxford University Press, 2011).
- [21] A. Suter and B. M. Wojek, *Physics Procedia* **30**, 69 (2012), [arXiv:1111.1569](#).
- [22] R. Sankar, I. Panneer Muthuselvam, G. J. Shu, W. T. Chen, S. K. Karna, R. Jayavel, and F. C. Chou, *CrystEngComm* **16**, 10791 (2014).
- [23] J. Sugiyama, M. Månsson, O. Ofer, K. Kamazawa, M. Harada, D. Andreica, A. Amato, J. H. Brewer, E. J. Ansaldo, H. Ohta, C. Michioka, and K. Yoshimura, *Physical Review B - Condensed Matter and Materials Physics* **84**, 1 (2011).
- [24] J. Sugiyama, M. Månsson, Y. Ikeda, T. Goko, K. Mukai, D. Andreica, A. Amato, K. Ariyoshi, and T. Ohzuku, *Physical Review B - Condensed Matter and Materials Physics* **79** (2009), [10.1103/PhysRevB.79.184411](#).
- [25] J. Sugiyama, H. Nozaki, M. Harada, K. Kamazawa, O. Ofer, M. Månsson, J. H. Brewer, E. J. Ansaldo, K. H. Chow, Y. Ikeda, Y. Miyake, K. Ohishi, I. Watanabe, G. Kobayashi, and R. Kanno, *Physical Review B - Condensed Matter and Materials Physics* **84**, 1 (2011).
- [26] J. Sugiyama, K. Mukai, Y. Ikeda, H. Nozaki, M. Månsson, and I. Watanabe, *Physical Review Letters* **103**, 1 (2009), [arXiv:0909.2921](#).
- [27] J. Sugiyama, H. Nozaki, M. Harada, K. Kamazawa, Y. Ikeda, Y. Miyake, O. Ofer, M. Månsson, E. J. Ansaldo, K. H. Chow, G. Kobayashi, and R. Kanno, *Physical Review B - Condensed Matter and Materials Physics* **85**, 1 (2012).
- [28] M. Månsson and J. Sugiyama, *Physica Scripta* **88** (2013), [10.1088/0031-8949/88/06/068509](#).
- [29] I. Umegaki, H. Nozaki, M. Harada, M. Månsson, H. Sakurai, I. Kawasaki, I. Watanabe, and J. Sugiyama, in *Proceedings of the 14th International Conference on Muon Spin Rotation, Relaxation and Resonance (μ SR2017)*, Vol. 011018 (2018) pp. 1–6.
- [30] H. Alloul, I. R. Mukhamedshin, A. V. Dooglav, Y. V. Dmitriev, V. C. Ciomaga, L. Pinsard-Gaudart, and G. Collin, *Physical Review B - Condensed Matter and Materials Physics* **85**, 1 (2012).
- [31] R. Siegel, J. Hirschinger, D. Carlier, S. Matar, M. Ménétrier, and C. Delmas, *Journal of Physical Chemistry B* **105**, 4166 (2001).
- [32] M. Medarde, M. Mena, J. L. Gavilano, E. Pomjakushina, J. Sugiyama, K. Kamazawa, V. Y. Pomjakushin, D. Sheptyakov, B. Batlogg, H. R. Ott, M. Månsson, and F. Juranyi, *Physical Review Letters* **110**, 1 (2013), [arXiv:1301.5827](#).